Acoustic-Hydraulic Nozzle for Fine Spray and High Performance

Olga Kudryashova *, Andrey Shalunov , Dmitry Genne , Roman Dorovskikh , Sergey Titov

Posted Date: 31 October 2023

doi: 10.20944/preprints202310.2036.v1

Keywords: Liquid atomization; ultrasound; acoustic-hydraulic nozzle; droplet dispersion; cavitation, critical mode.

Article

Acoustic-Hydraulic Nozzle for Fine Spray and High Performance

Olga Kudryashova [1,*], Andrey Shalunov [2], Dmitry Genne [3], Roman Dorovskikh [4] and Sergey Titov [5]

[1] Facility of Physics and Technology, Tomsk State University, 634050 Tomsk, Russia; olgakudr@inbox.ru
[2] Biysk Technological Institute (branch) of Polzunov Altai State Technical University, 659305 Biysk, Russia; shalunov@bti.secna.ru
[3] Biysk Technological Institute (branch) of Polzunov Altai State Technical University, 659305 Biysk, Russia; gdv@bti.secna.ru
[4] Biysk Technological Institute (branch) of Polzunov Altai State Technical University, 659305 Biysk, Russia; dorovskih_roman@mail.ru
[5] Institute for problems of Chemical and Energetic Technologies of the Siberian Branch of the RAS; titov.sergey.s@gmail.com
* Correspondence: olgakudr@inbox.ru; Tel.: +79059245444

Featured Application: The acoustic-hydraulic nozzle can be used in technological tasks where both high droplet dispersion and high productivity of creating an aerosol flow are required.

Abstract: Spray technology is widely used in various industries, including medicine, food production, mechanical engineering, and nanopowder manufacturing. Achieving high dispersion and a narrow particle size distribution is crucial for many applications. Ultrasonic spraying is commonly used to achieve this. On other hand, hydraulic nozzles provide high atomization performance. Combining these two technologies promises to offer significant benefits, but the complex processes that occur simultaneously in such a device require careful study. This work proposes a fundamental design for an acoustic-hydraulic nozzle and investigates the physical processes when a liquid is sprayed using this nozzle, both theoretically and experimentally. The study identifies the critical modes of spraying and confirms that the simultaneous use of ultrasound and hydraulic pressure can produce a fine spray (droplet size less than 50 μm) with high productivity (5-10 ml/s). This approach has significant potential for modern industries and technologies.

Keywords: liquid atomization; ultrasound; acoustic-hydraulic nozzle; droplet dispersion; cavitation; critical mode

1. Introduction

Liquid atomization is a crucial manufacturing process that finds application in a diverse range of fields. Over time, numerous spraying methods and devices have been developed based on different physical principles, including hydraulic, pneumatic, and mechanical, and their combinations [1].

The hydraulic atomization of liquid is the most conventional method, wherein the liquid is converted into droplets when it flows through the nozzle hole under high pressure. This process is extensively employed in industries and agriculture for the application of various solutions, chemicals, fertilizers, etc. [2].

One innovative spraying method is ultrasonic spraying, which uses ultrasonic vibrations to create fine droplets of liquid. This method is widely used in industrial applications such as fuel combustion [3], nanoemulsification emulsification [4], wet dust removal [5], air humidification [6], atomization pyrolysis [7], and metal powder atomization [8]. The advantage of this method is the stable and predictable relationship between operating parameters, spraying speed, and droplet diameter [9,10]. Additionally, ultrasonic spraying results in the narrowest droplet size distribution compared to other spraying methods. However, the downside of using ultrasonic spraying is low

Preprints (www.preprints.org) | NOT PEER-REVIEWED | Posted: 31 October 2023 doi:10.20944/preprints202310.2036.v1

productivity, and the higher the droplet dispersion, the lower the productivity of droplet creation [11]. For example, when generating droplets with a diameter of up to 10 μm, productivity can be as low as 0.1 ml/(s·cm²).

On the other hand, hydraulic spraying makes it possible to obtain an aerosol with high productivity (tens of ml/s). However, with this spraying method, the droplet dispersion is low, and the higher the productivity, the lower the droplet dispersion (for example, 1000 microns at 25 l/min). Although many combined spraying methods have been created [1], no attempts have been made to combine ultrasonic and hydraulic spraying. This may be due to the complexity of organizing such spraying and the physical processes accompanying it.

We propose a model scheme for the design of an acoustic-hydraulic nozzle with the goal of combining the advantages of both methods and achieving high droplet dispersion with high productivity. The purpose of this work is to experimentally and theoretically study acoustic-hydraulic spraying. Our tasks are to determine the spraying mechanisms, conditions, and operating parameters of an acoustic-hydraulic nozzle depending on the conditions and physical and chemical properties of the liquid.

2. Materials and Methods

We are considering the following design of an acoustic-hydraulic nozzle (Figure 1). In direction 1, liquid is supplied to cylindrical tube 2 under pressure p. The ultrasonic emitter 3 oscillates along the axis of the tube. In zone 4, the liquid cavitates under the influence of ultrasonic radiation and flows out of outlet 5 in the form of a spray of drops 6. The outlet is located opposite the end surface of the emitter at a distance of 7.

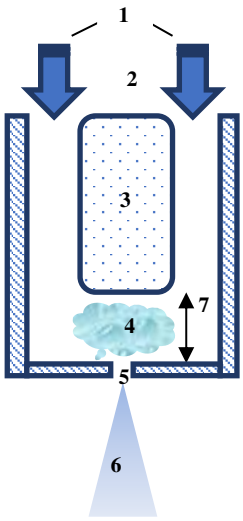

Figure 1. Acoustic-hydraulic nozzle scheme: 1 – liquid supply direction, 2 – cylindrical tube, 3 – ultrasonic emitter, 4 – cavitation zone, 5 – outlet, 6 – liquid drops, 7 – cavitation zone height L.

The main geometric parameters of the nozzle used in the calculations:

- the area of the end part of the ultrasonic emitter 3 – S_1,
- the area of the outlet 5 – S_2,
- the cross-sectional area of the tube 2 – S_3,
- the height of the cavitation zone (distance from the surface of emitter to the outlet) 7 – L.

Using a nozzle, we sprayed the settled tap water. Droplet size was measured using a Spraytec instrument (Malvern Instruments, UK). The operating principle of the measuring system is based on laser diffraction. The Spraytec system allows us to measure particle dispersion with a frequency of up to 10 kHz in the range from 0.1 to 2000 microns. An example of a histogram and statistical characteristics of the particle size distribution obtained using the Spraytec system is shown in Figure

Preprints (www.preprints.org) | NOT PEER-REVIEWED | Posted: 31 October 2023 doi:10.20944/preprints202310.2036.v1

2. Statistical data measured using Spraytec system for different pressure values at an intensity of 70 W/cm² are shown in the Appendix A (Figures A1–A8).

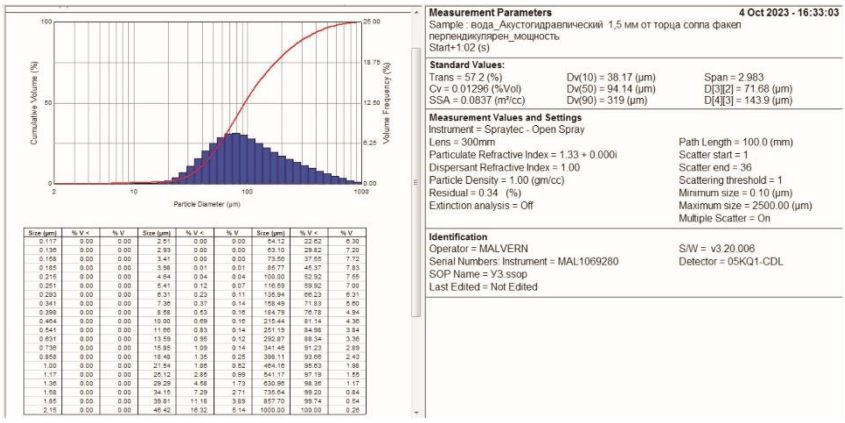

Figure 2. Example of a histogram and statistical characteristics of the particle size distribution formed using the developed nozzle (obtained using Spraytec).

To describe the mechanisms of sputtering and the physical processes occurring during this process, we used mathematical modeling methods.

3. Mathematical model of the acoustic-hydraulic nozzle

3.1. Hydrodynamic processes. Hydrodynamic cavitation threshold

In the system under consideration, processes occur that involve the movement of fluid under the influence of hydrostatic pressure and ultrasonic vibrations. Under certain conditions, both hydrodynamic cavitation and ultrasonic cavitation processes can occur. Let's consider these conditions.

The hydrodynamic cavitation threshold occurs at a certain fluid supply pressure:

$$\mathrm{X} = \frac{(p - p_s)(1 - \varepsilon^2)}{\varepsilon^2 (p - p_a)} \le 1, \tag{1}$$

where p is the hydrostatic pressure of the liquid flow, p_s is the vapor pressure of the liquid, p_a is the atmospheric pressure, $\varepsilon = S_2/S_1$, S_1 is the cross-sectional area of the cavitation zone, S_2 is the area of the outlet.

This expression was obtained by jointly solving the continuity equation and the Berlulli equation in the inlet section into the cavitation zone:

$$V_x = \sqrt{\frac{2(p - p_a)}{\rho(1 - \varepsilon^2)}}, \qquad V_1 = \varepsilon V_x. \tag{2}$$

where V_1 is the flow velocity in the cavitation zone, V_x is the flow velocity after the outflow, ϱ is the density of the liquid.

The hydrodynamic cavitation number is defined as $\mathrm{X} = \frac{2(p - p_s)}{\rho V_1^2}$. For X > 1, the flow regime is pre-cavitation; for X < 1, developed cavitation is observed. From equation (1) we obtain the cavitation pressure threshold:

$$p_{cr} = \frac{p_a \xi - p_s}{\xi - 1}, \tag{3}$$

Preprints (www.preprints.org) | NOT PEER-REVIEWED | Posted: 31 October 2023 doi:10.20944/preprints202310.2036.v1

where $\xi = \frac{\varepsilon^2}{1-\varepsilon^2}$. At pressures above p_{cr}, hydrodynamic cavitation occurs.

It should be noted that the pressure p_1 in the cavitation zone differs from the liquid pressure at the inlet to the structure p. By solving the system of continuity and Bernoulli equations in two sections – at the entrance and exit to the cavitation zone – we obtain an expression for the pressure in the cavitation zone:

$$p_1 = p + \xi(p - p_a)\left(\left(\frac{S_1}{S_0}\right)^2 - 1\right), \quad (4)$$

where $S_0 = S_3 - S_1$ is the cross-sectional area of the annular part of the structure (flow area before entering the cavitation zone).

The volumetric flow rate of the liquid is expressed by the equation:

$$Q = V_x \cdot S_2 = S_2\sqrt{\frac{2(p - p_a)}{\rho(1-\varepsilon^2)}}. \quad (5)$$

We will evaluate the performance of the nozzle under consideration in accordance with expression (5).

3.2. Ultrasonic exposure. Acoustic cavitation threshold

In the cavitation zone of the structure, between the end of the emitter and the outlet, conditions for the development of cavitation are created. Even with a low intensity of ultrasonic exposure, bubbles filled with water vapor appear in the liquid in this area. The size of the bubbles depends significantly on the intensity of the sound field:

$$D_c \sim \frac{2}{\omega}\sqrt{\frac{I}{\rho c}}. \quad (6)$$

This expression is obtained from the following considerations. The amplitude of the displacement of liquid particles in a sound wave A is related to the ultrasound intensity I [W/m²], the speed of sound c and the frequency ω by the known relationship: $I = \frac{A^2\omega^2 c\rho}{2}$. When a wave passes through a liquid in the unloading phase, discontinuities of size A are formed in it, and in the compression phase, gas bubbles with a diameter D_c are formed at the site of these discontinuities. The diameter of the cavitation bubble corresponds to the size of the gap A.

From equation (6) it follows that the higher the ultrasound intensity, the larger the diameter of the bubbles formed. In this case, with the development of cavitation, the wave resistance $W_l = \rho \cdot c$ decreases significantly in accordance with the increase in the volume fraction of vapors in the liquid [12], which means that the diameter of the bubbles also increases.

Let us consider the following qualitative physical picture of the development of cavitation. At a minimum intensity of ultrasound of I_{min} in the liquid volume, cavitation bubbles in the amount of N_0 are formed on existing inhomogeneities (cavitation nuclei), which, in accordance with (6), will have a minimum size of ~ $I_{min}^{1/2}$. Their number does not increase with increasing intensity, but their size, and, accordingly, volume gradually increases. The mode of developed cavitation occurs when a certain bubble size D_{cr} is reached. In this case, the volume of bubbles Wg becomes comparable to the volume of liquid W_w, and the continuity of the medium is disrupted. In the mode of developed cavitation, as confirmed experimentally, the cavitation coefficient K = W_g / W_w remains unchanged and corresponds to approximately 0.2 ÷ 0.3 [13]. This limit is probably determined by the strength properties of the liquid. The volume of liquid in our case is determined as $W_w = S_1 \cdot L$. If the ultrasound intensity increases further, the size of the bubbles will continue to increase and their number will decrease. Let us denote the intensity corresponding to the mode of developed cavitation as I_{cr}. We will define this regime as critical and find the conditions for its occurrence.

Preprints (www.preprints.org) | NOT PEER-REVIEWED | Posted: 31 October 2023 doi:10.20944/preprints202310.2036.v1

With a further increase in intensity at a constant total volume of bubbles, their number N decreases in accordance with a power law with an exponent of 3/2. This means that the number of bubbles drops quickly at first and then weaker. We can conditionally select an intensity value I_{max} such that the change in the number of bubbles relative to the change in intensity is small. That is, a further increase in intensity practically does not affect the number of bubbles in the liquid. It can be shown that the bubble diameter in this regime will be approximately e times greater than D_{cr}, and the intensity $I_{max} \sim e^2 \cdot I_{cr}$.

The above considerations correspond to the case of the absence of excess hydrostatic pressure in the liquid. The size of the bubbles, of course, also depends on the pressure in the liquid. According to the Boyle-Mariotte law:

$$D_c^3 \sim \frac{1}{p}. \tag{7}$$

Thus, the critical volume of bubbles will be proportional to the ratio of the critical value of intensity to the power of 3/2 and pressure:

$$D_{cr}^3 \sim \frac{I_{cr}^{3/2}}{p}. \tag{8}$$

This means that, depending on the hydrostatic pressure, a noticeable cavitation effect from ultrasonic exposure will be observed at different values of ultrasound intensity: the higher the pressure, the higher the ultrasound intensity required for developed cavitation and vice versa.

As follows from dependencies (6) and (7), the diameter of the cavitation bubble is proportional to the square root of the ultrasound intensity and inversely proportional to the ultrasound frequency and the cube root of the hydrostatic pressure:

$$D_c = \frac{2}{\omega}\sqrt[3]{\frac{p_a}{p}}\sqrt{\frac{I}{\rho c}}. \tag{9}$$

We will consider the critical diameter D_{cr} to be a free parameter of the model. In accordance with it, at a given hydrostatic pressure, the critical (threshold) intensity of developed cavitation is determined:

$$I_{cr} = \frac{D_{cr}^2 \omega^2 \rho c}{4}\left(\frac{p}{p_a}\right)^{2/3}. \tag{10}$$

Note that, in accordance with equation (10), the critical intensity will be proportional to the hydrostatic pressure to the power of 2/3. The higher the pressure in the liquid, the higher the required ultrasound intensity for the onset of developed cavitation.

The number of bubbles will be determined as the ratio of the gas volume to the volume of one bubble, calculated according to formula (9):

$$N = \frac{4W_g}{\pi D^3} = \frac{KW_w}{2\pi}\left(\frac{p}{p_a}\right)\omega^3 (\rho c)^{3/2} I^{-3/2}. \tag{11}$$

As will be shown below, the size of the droplets depends significantly on the size of the bubbles and their number.

3.3. Droplet size upon expiration of cavitated liquid

What happens to the bubble after its nucleation? As shown in [13], under conditions of continuous flow, cavitation bubbles do not collapse, but only grow.

It can be assumed that when the cavitated liquid flows into the atmosphere, each bubble will carry with it a layer of liquid, inversely proportional to the number of bubbles: W_w/N. This volume will determine the maximum volume of the drop. Then, taking into account (9) and (11), its diameter is:

Preprints (www.preprints.org) | NOT PEER-REVIEWED | Posted: 31 October 2023 doi:10.20944/preprints202310.2036.v1

$$D_0 = \frac{2}{\omega}\sqrt[3]{\frac{p_a}{\mathrm{K}p}}\sqrt{\frac{I}{\rho c}} = \frac{D_c}{\sqrt[3]{\mathrm{K}}}. \quad (12)$$

Thus, the maximum droplet diameter is 1.5-1.7 times larger than the diameter of the cavitation bubble. This model does not take into account the surface energy of the liquid carried by the cavitation bubble. On the other hand, a gas bubble surrounded by liquid, when exposed to atmospheric pressure, will behave like a soap bubble. It will expand to a certain maximum size, determined by surface tension forces, and only then will it collapse into fragments with sizes on the order of the thickness of the liquid layer at that moment [14]. Let's take a closer look at this model.

Since the outflow occurs quickly, the cavitation expansion can be considered adiabatic:

$$\frac{D_{\max}}{D_c} = \left(\frac{p}{p_{\min}}\right)^{\frac{1}{3\gamma}}, \quad (13)$$

where γ is the adiabatic index of liquid vapor, $p_{\min}$ is the minimum pressure in the bubble at the moment of destruction, $D_{\max}$ is the maximum diameter of the bubble before destruction. The bubble expands as long as the surface energy of the liquid layer $\sigma \cdot S_c$ is greater than the internal energy of the vapor inside it $p_{\min} W_c$, where W_c is the volume of the cavitation bubble, S_c is its surface, σ is the surface tension. When these energies become equal, it will collapse. From here we obtain the minimum pressure in the bubble at the moment of destruction:

$$p_{\min} = \frac{6\sigma}{D_{\max}}. \quad (14)$$

Solving equations (9, 13, 14) together we obtain the value of the bubble diameter before destruction:

$$D_{\max} = \left(\frac{p}{6\sigma}\right)^{\frac{1}{3\gamma-1}} D_c^{\frac{3\gamma}{3\gamma-1}}. \quad (15)$$

The volume of liquid that the bubble carried with it is $\frac{\pi D_0^3}{6}$, where the diameter D_0 is determined by expression (12). Let us denote the outer diameter of the bubble before destruction by D_{end}. Then from the law of conservation of mass it follows: $D_0^3 - D_c^3 = D_{end}^3 - D_{\max}^3$. From here

$$D_{end} = \sqrt[3]{D_{\max}^3 + D_c^3(1/\sqrt[3]{\mathrm{K}} - 1)}. \quad (16)$$

It can be assumed that the minimum droplet size will be equal to the thickness of the liquid layer upon destruction of the cavitation bubble. The thickness of the water layer at the moment of destruction, and therefore the size of the droplets, will be $D_{\text{drop}} = (D_{end} - D_{\max}) / 2$. Or, taking into account (13):

$$D_{drop} = k\left(\sqrt[3]{D_{\max}^3 + D_c^3(1/\sqrt[3]{\mathrm{K}} - 1)} - D_{\max}\right)/2. \quad (17)$$

A joint solution of equations (9), (15) and (17) will give an estimate of the minimum size of droplets formed during spraying, depending on the characteristics of ultrasonic influence, pressure and properties of the liquid. In equation (17), the coefficient k is introduced, which is a free parameter of the model. If $k = 1$, then equation (17) gives a lower estimate for the droplet size. However, the size of all droplets will not be minimal; a spectrum of particle sizes up to the maximum D_0 is realized.

Thus, we proposed a mathematical model of the processes occurring in an acoustic-hydraulic nozzle and theoretically determined the critical modes, productivity and droplet size of the resulting aerosol. The model has two free parameters that need to be determined experimentally – D_{cr} and k. If our reasoning is correct, then the experimental dependences will have a character corresponding to that described theoretically, including the critical nature of spaying.

Preprints (www.preprints.org) | NOT PEER-REVIEWED | Posted: 31 October 2023 doi:10.20944/preprints202310.2036.v1

4. Results and discussion

4.1. Experimental results. Droplet sizes, critical spraying mode

The geometric parameters of the nozzle used in the experiment are as follows:

- outlet area S_1 = 0.38 mm²;
- area of the cavitation zone S_2 = 50 mm²;
- cross-sectional area of the tube S_3 = 78.5 mm²;
- height of the cavitation zone – L = 1.5 cm.

The frequency of ultrasonic radiation was ω = 22.5 kHz, the intensity varied in the range from 30 to 100 W/cm², the hydraulic pressure p was from 200 kPa to 900 kPa.

At a fixed intensity, the following picture was observed with increasing pressure. Up to a certain pressure p_{cr}, the resulting droplets were relatively large in size (hundreds of micrometers), then the droplet size decreased significantly and remained approximately constant with further increases in pressure (Table 1). This spraying mode corresponds to cavitation flow and was established at pressure p_{cr} and intensity I_{cr}. The critical values of the intensity I_{cr} depending on the pressure are given in Table 2. With increasing intensity, the critical pressure p_{cr} of the transition to the cavitation mode becomes higher, and vice versa, with increasing pressure, a higher intensity of the transition to the cavitation mode is required.

Table 1. Sauter mean diameter of liquid droplets D_{32} (μm) depending on pressure and ultrasound intensity.

p/p_a		**2**	**3**	**4**	**5**	**6**	**7**	**8**	**9**
I_{cr}, **W/cm²**	**70**	190	146	126	111	71	44	39	42
	80	217	139	122	98	73	77	35	28

It should be noted that in the absence of ultrasound, the characteristic droplet size is of the order of 500 μm and higher in a given pressure range.

Table 2. Critical pressure depending on ultrasound intensity.

p/p_a	**2**	**3**	**4**	**5**	**6**	**7**	**8**	**9**
I_{cr}, **W/cm²**	26	31	49	55	82	86	104	112

Figure 3 shows the operation of the experimental setup at the moment the cavitation mode is established.

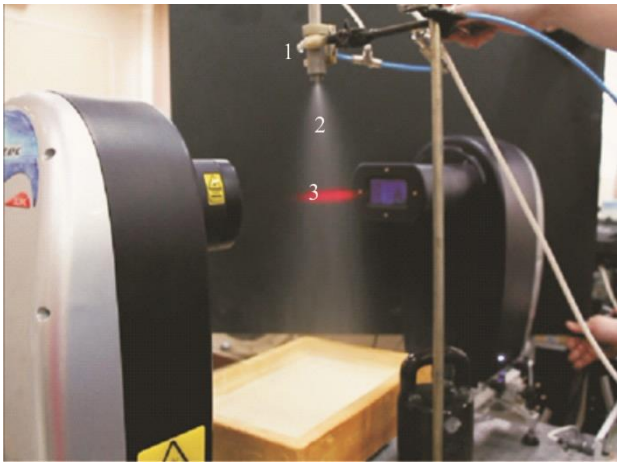

Figure 3. Operation of the experimental setup when the cavitation outflow mode is established: 1 – nozzle, 2 – liquid drops, 3 – laser probe beam.

The productivity (volume flow rate) of the liquid increased with pressure in all experiments, however, when passing through the critical point (p_{cr}, I_{cr}), the nature of the growth changed (Figure

Preprints (www.preprints.org) | NOT PEER-REVIEWED | Posted: 31 October 2023 doi:10.20944/preprints202310.2036.v1

4). In any case, sprayimg without the use of ultrasound occurred at a slightly higher speed than with ultrasound (curve "w/o US" in Figure 4).

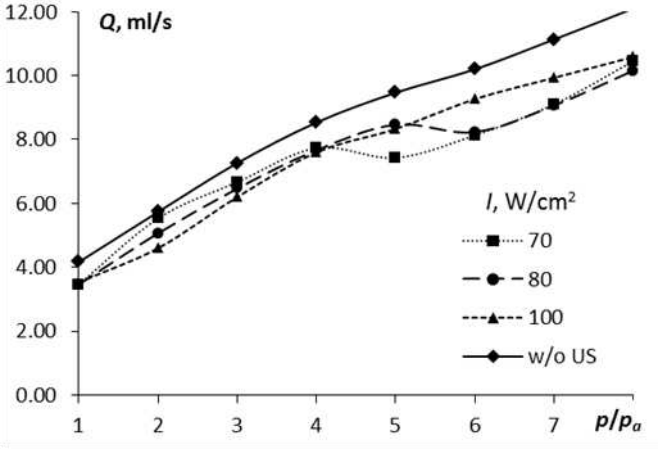

Figure 4. Experimental dependence of volume flow on pressure and ultrasound intensity.

Apparently, the decrease in flow rate is associated with an increase in the hydraulic resistance of the nozzle, due to the large volume of cavitation bubbles in the mode of developed cavitation.

4.2. Calculation results. Comparison of theoretical and experimental results

4.2.1. Possibility of hydrodynamic cavitation

Figure 5 a shows the dependence of the cavitation number on pressure for different values of the geometric parameter ε, and Figure 5 b shows the dependence of the critical pressure, above which cavitation mode may occur in the structure under consideration.

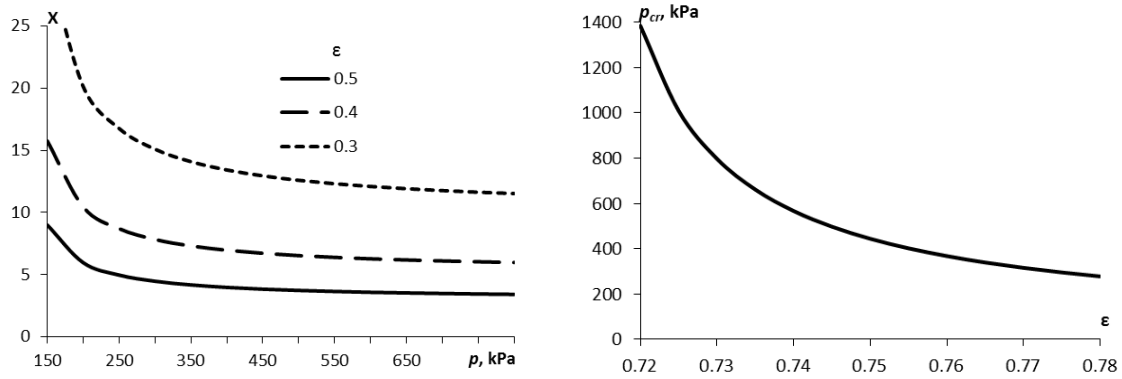

(**a**) (**b**)

Figure 5. The number of hydrodynamic cavitation depending on pressure (a) and the dependence of the critical pressure of hydrodynamic cavitation on the parameter ε (b).

Based on the conditions of the problem, our design does not implement the hydrodynamic cavitation mode, since the parameter ε = 0.005 is significantly less than those for which cavitation is possible at relatively low pressures.

The volumetric flow rate of liquid in the nozzle is shown in Figure 6. It should be noted that the geometric parameter does not have a significant effect on the flow rate. The above calculation does not take into account ultrasonic influence. As can be seen from the experiment (Figure 4) and will be shown theoretically below, ultrasonic action reduces the outflow velocity and volume flow.

Preprints (www.preprints.org) | NOT PEER-REVIEWED | Posted: 31 October 2023 doi:10.20944/preprints202310.2036.v1

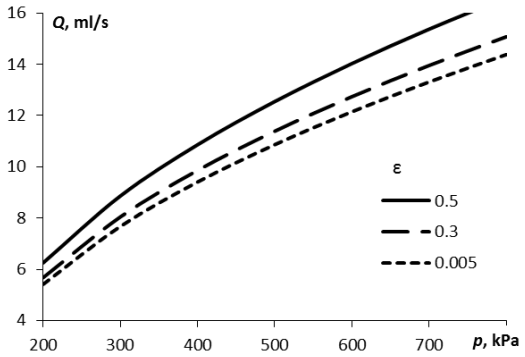

Figure 6. Volumetric fluid flow depending on pressure and geometric parameter ε.

4.2.2. Ultrasonic cavitation

Figure 7 shows the dependence of the diameter of cavitation bubbles on pressure and frequency of exposure at different intensity values.

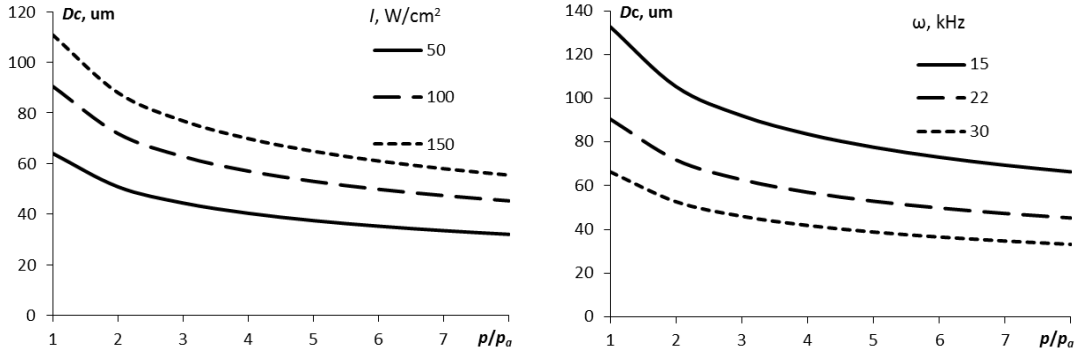

Figure 7. Dependence of the size of cavitation bubbles on pressure for different values of intensity (a, frequency $\omega = 22.5$ kHz) and frequency (b, $I = 100$ W/cm²).

With increasing pressure, the size of the bubbles decreases in accordance with equation (9). Also, the size of the bubbles decreases with increasing frequency of exposure, but increases with increasing intensity.

The free parameter of the problem is D_{cr}. When compared with experimental data, it was found that its value is approximately 30 μm. Figure 8 shows the dependence of the critical intensity of ultrasonic exposure, calculated in accordance with equation (10) together with experimental values (Table 2).

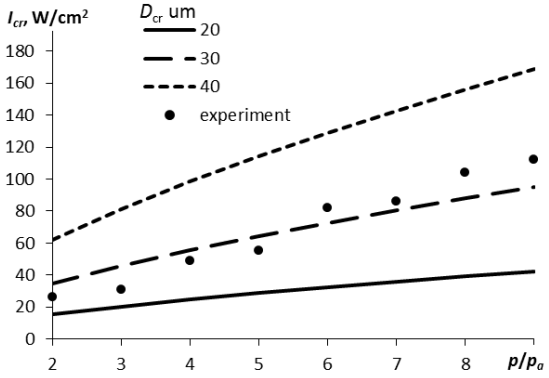

Figure 8. Critical intensity as a function of pressure for different values of the critical bubble size.

Preprints (www.preprints.org) | NOT PEER-REVIEWED | Posted: 31 October 2023 doi:10.20944/preprints202310.2036.v1

4.2.3. Droplet size

The droplet size calculated in accordance with equation (17) (free parameter $k = 300$) is shown in Figure 9.

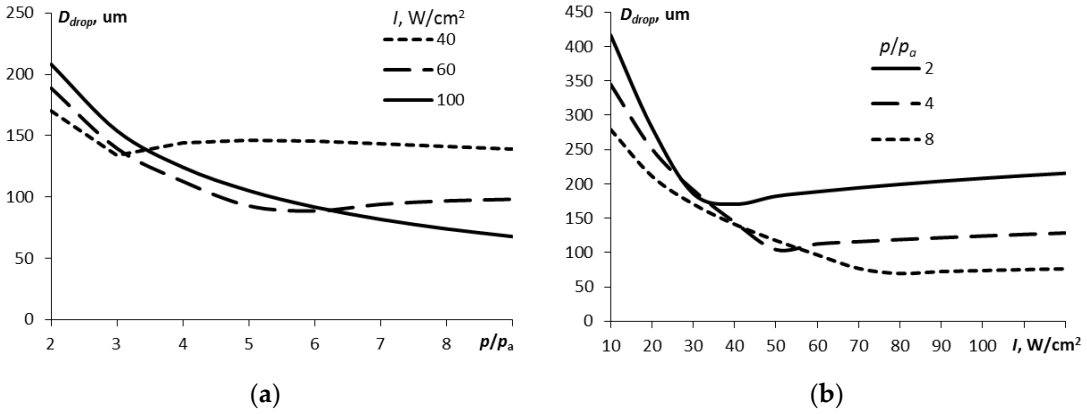

Figure 9. Characteristic size of droplets depending on pressure (a) and intensity (b).

Figure 9 demonstrates the critical nature of the occurring phenomena. Upon transition to the cavitation outflow mode, the droplet size becomes minimal (and with a further increase in pressure or intensity, it only slightly increases). In this case, the critical conditions in terms of pressure and intensity correspond to the observed ones: the higher the pressure, the higher the intensity required for the transition to the cavitation outflow regime, and vice versa.

The free model parameter $k = 300$ (equation (17)) was chosen based on comparison with experiment. Figure 10 shows experimental points (Table 1) and calculated curves for droplet size.

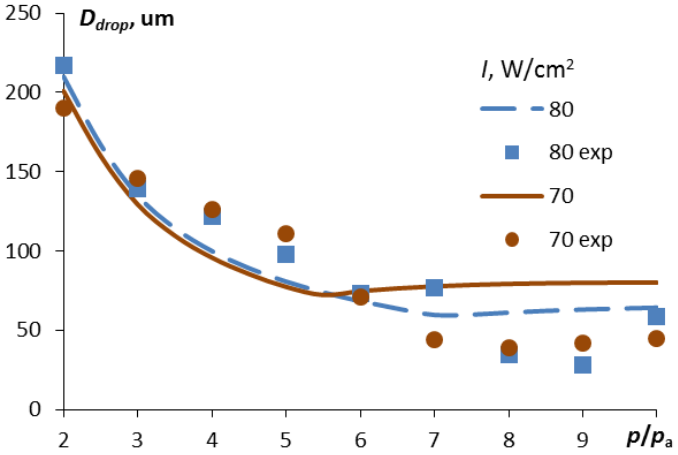

Figure 10. Experimental and calculated dependences of the characteristic droplet size on the pressure drop for different levels of ultrasound intensity.

The size of droplets during ultrasonic spraying using the capillary wave mechanism is estimated using Lang's equation [15]:

$$d_{us} = 0.34\sqrt[3]{\frac{8\pi\sigma}{\rho\omega^2}}. \quad (18)$$

Thus, the higher the frequency, the smaller the droplet. With the classical method of ultrasonic spraying, the droplet size at a frequency of 22.5 kHz, the Sauter mean diameter of the droplets D_{32} = 100...120 μm. Moreover, the 22.5 kHz frequency used in our design is energetically more favorable than higher frequencies.

Preprints (www.preprints.org) | NOT PEER-REVIEWED | Posted: 31 October 2023 doi:10.20944/preprints202310.2036.v1

When spraying with hydraulic nozzles, the size of the droplets depends on the liquid pressure in the nozzle: the higher the pressure, the smaller the droplets. On the other hand, the flow rate (or volumetric flow rate) of the liquid is important: the lower the flow rate, the higher the dispersion [16]. The corresponding empirical formulas depend on the fundamental design of the nozzle, but at a pressure of 8...9 atm and a volume flow rate of 10...12 ml/s, the droplet diameter does not decrease less than 100...150 μm (at lower pressure values, the droplet size is significantly larger). In our design of an acoustic-hydraulic nozzle, when switching to cavitation mode, a finer spray is achieved (D_{32} < 50 μm) with a productivity almost equal to that of a hydraulic nozzle. Figure 11 shows the calculated and experimental dependences of the volumetric flow rate of liquid at two intensity levels and in the absence of ultrasonic influence.

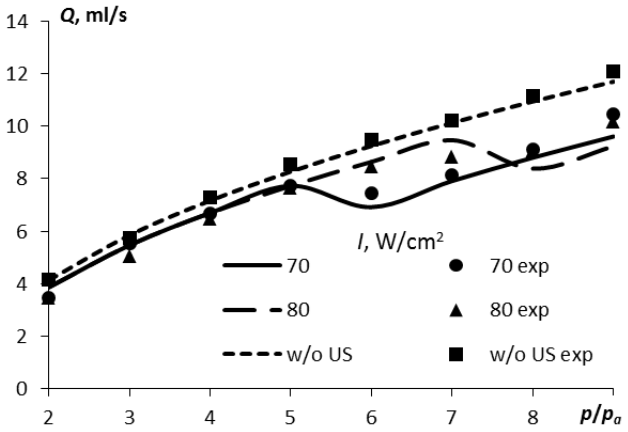

Figure 11. Volumetric flow rate of liquid - calculated curves and experimental points.

As can be seen from the figure, both theory and experiment show the critical nature of the flow depending on pressure and ultrasound intensity. During the transition to the cavitation mode, the volume flow rate decreases, and then the flow rate increases again with pressure. At the same time, the reduction in flow rate in cavitation mode compared to the case of the absence of ultrasonic influence is not significant (5-10%). Meanwhile, in the cavitation mode, the dispersion of droplets is significantly higher compared to hydraulic spraying.

5. Conclusions

The development of new liquid atomization devices and methods that can produce a fine spray at high throughput is of significant interest for various technological applications. In this study, we proposed and investigated the design of an acoustic-hydraulic nozzle that combines the benefits of the hydraulic spray method (high productivity) and ultrasonic spraying (high droplet dispersion). The proposed theoretical model was validated through experimental data, and we identified critical conditions for intensity and pressure, which are the controlling parameters of the device. These conditions enable the implementation of the cavitation spray mode and achieve the desired process characteristics.

Our results demonstrate that the proposed design can achieve droplet sizes of less than 50 microns with a productivity of about 5-10 ml/s at an exposure frequency of 22.5 kHz when creating conditions of cavitation spraying. Such a small droplet size at the used ultrasonic frequency of 22.5 kHz and the achieved spraying productivity is not attainable by either ultrasonic or hydraulic spraying methods separately, as demonstrated theoretically and experimentally.

Overall, our findings suggest that the acoustic-hydraulic nozzle has significant potential in various technological applications that require high-throughput, fine spray production. Further studies can explore the optimization of the device's parameters to achieve even better performance.

Author Contributions: Conceptualization, A.S. and O.K.; methodology, D.G.; investigation, R.D.; resources, S.T.; writing—original draft preparation, O.K.; writing—review and editing, supervision, A.S.; project

Preprints (www.preprints.org) | NOT PEER-REVIEWED | Posted: 31 October 2023 doi:10.20944/preprints202310.2036.v1

administration, A.S.; funding acquisition, S.T. All authors have read and agreed to the published version of the manuscript."

Funding: This study was carried out with a grant from the Russian Science Foundation (project №19-19-00121).

Conflicts of Interest: The authors declare no conflict of interest.

Appendix A

Size (μm)	% V <	% V	Size (μm)	% V <	% V	Size (μm)	% V <	% V
0.117	0.00	0.00	2.51	0.02	0.00	54.12	3.61	1.46
0.136	0.00	0.00	2.93	0.02	0.00	63.10	5.49	1.89
0.158	0.00	0.00	3.41	0.02	0.00	73.56	7.77	2.28
0.185	0.00	0.00	3.98	0.02	0.00	85.77	10.36	2.59
0.215	0.00	0.00	4.64	0.02	0.00	100.00	13.21	2.85
0.251	0.00	0.00	5.41	0.02	0.00	116.59	16.29	3.08
0.293	0.00	0.00	6.31	0.02	0.00	135.94	19.65	3.36
0.341	0.00	0.00	7.36	0.02	0.00	158.49	23.43	3.78
0.398	0.00	0.00	8.58	0.02	0.00	184.79	27.80	4.37
0.464	0.00	0.00	10.00	0.02	0.00	215.44	32.95	5.15
0.541	0.00	0.00	11.66	0.02	0.00	251.19	39.03	6.07
0.631	0.00	0.00	13.59	0.02	0.00	292.87	46.06	7.03
0.736	0.00	0.00	15.85	0.02	0.00	341.46	53.95	7.89
0.858	0.00	0.00	18.48	0.02	0.00	398.11	62.43	8.48
1.00	0.00	0.00	21.54	0.02	0.00	464.16	71.12	8.69
1.17	0.00	0.00	25.12	0.02	0.00	541.17	79.51	8.39
1.36	0.00	0.00	29.29	0.15	0.12	630.96	87.08	7.56
1.58	0.00	0.00	34.15	0.48	0.34	735.64	93.29	6.21
1.85	0.02	0.02	39.81	1.12	0.64	857.70	97.71	4.42
2.15	0.02	0.00	46.42	2.15	1.03	1000.00	100.00	2.29

Figure A1. Statistical characteristics of the particle size distribution for p = 200 kPa.

Size (μm)	% V <	% V	Size (μm)	% V <	% V	Size (μm)	% V <	% V
0.117	0.00	0.00	2.51	0.02	0.00	54.12	6.42	2.45
0.136	0.00	0.00	2.93	0.02	0.00	63.10	9.51	3.10
0.158	0.00	0.00	3.41	0.02	0.00	73.56	13.15	3.64
0.185	0.00	0.00	3.98	0.02	0.00	85.77	17.18	4.03
0.215	0.00	0.00	4.64	0.02	0.00	100.00	21.45	4.27
0.251	0.00	0.00	5.41	0.02	0.00	116.59	25.86	4.41
0.293	0.00	0.00	6.31	0.02	0.00	135.94	30.39	4.53
0.341	0.00	0.00	7.36	0.02	0.00	158.49	35.12	4.73
0.398	0.00	0.00	8.58	0.02	0.00	184.79	40.16	5.04
0.464	0.00	0.00	10.00	0.02	0.00	215.44	45.63	5.47
0.541	0.00	0.00	11.66	0.02	0.00	251.19	51.61	5.98
0.631	0.00	0.00	13.59	0.02	0.00	292.87	58.09	6.48
0.736	0.00	0.00	15.85	0.02	0.00	341.46	64.94	6.85
0.858	0.00	0.00	18.48	0.02	0.00	398.11	71.94	7.00
1.00	0.00	0.00	21.54	0.02	0.00	464.16	78.79	6.86
1.17	0.00	0.00	25.12	0.09	0.07	541.17	85.18	6.39
1.36	0.02	0.02	29.29	0.37	0.29	630.96	90.76	5.58
1.58	0.02	0.00	34.15	1.02	0.65	735.64	95.25	4.48
1.85	0.02	0.00	39.81	2.18	1.16	857.70	98.38	3.14
2.15	0.02	0.00	46.42	3.96	1.78	1000.00	100.00	1.62

Figure A2. Statistical characteristics of the particle size distribution for p = 300 kPa.

Size (μm)	% V <	% V	Size (μm)	% V <	% V	Size (μm)	% V <	% V
0.117	0.00	0.00	2.51	0.00	0.00	54.12	9.67	3.03
0.136	0.00	0.00	2.93	0.00	0.00	63.10	13.26	3.59
0.158	0.00	0.00	3.41	0.00	0.00	73.56	17.26	4.00
0.185	0.00	0.00	3.98	0.00	0.00	85.77	21.50	4.24
0.215	0.00	0.00	4.64	0.00	0.00	100.00	25.83	4.33
0.251	0.00	0.00	5.41	0.01	0.01	116.59	30.18	4.35
0.293	0.00	0.00	6.31	0.03	0.02	135.94	34.56	4.38
0.341	0.00	0.00	7.36	0.06	0.04	158.49	39.07	4.51
0.398	0.00	0.00	8.58	0.13	0.07	184.79	43.86	4.79
0.464	0.00	0.00	10.00	0.22	0.09	215.44	49.06	5.20
0.541	0.00	0.00	11.66	0.30	0.08	251.19	54.76	5.70
0.631	0.00	0.00	13.59	0.30	0.00	292.87	60.93	6.17
0.736	0.00	0.00	15.85	0.30	0.00	341.46	67.44	6.51
0.858	0.00	0.00	18.48	0.31	0.01	398.11	74.07	6.63
1.00	0.00	0.00	21.54	0.42	0.11	464.16	80.51	6.44
1.17	0.00	0.00	25.12	0.74	0.32	541.17	86.45	5.94
1.36	0.00	0.00	29.29	1.39	0.65	630.96	91.60	5.15
1.58	0.00	0.00	34.15	2.52	1.13	735.64	95.69	4.10
1.85	0.00	0.00	39.81	4.25	1.73	857.70	98.54	2.85
2.15	0.00	0.00	46.42	6.63	2.38	1000.00	100.00	1.46

Figure A3. Statistical characteristics of the particle size distribution for p = 400 kPa.

Size (μm)	% V <	% V	Size (μm)	% V <	% V	Size (μm)	% V <	% V
0.117	0.00	0.00	2.51	0.00	0.00	54.12	11.87	3.46
0.136	0.00	0.00	2.93	0.00	0.00	63.10	15.91	4.04
0.158	0.00	0.00	3.41	0.00	0.00	73.56	20.37	4.46
0.185	0.00	0.00	3.98	0.01	0.01	85.77	25.07	4.70
0.215	0.00	0.00	4.64	0.03	0.02	100.00	29.86	4.80
0.251	0.00	0.00	5.41	0.06	0.04	116.59	34.67	4.81
0.293	0.00	0.00	6.31	0.11	0.05	135.94	39.48	4.81
0.341	0.00	0.00	7.36	0.18	0.06	158.49	44.36	4.88
0.398	0.00	0.00	8.58	0.24	0.06	184.79	49.41	5.05
0.464	0.00	0.00	10.00	0.29	0.05	215.44	54.70	5.29
0.541	0.00	0.00	11.66	0.33	0.04	251.19	60.28	5.57
0.631	0.00	0.00	13.59	0.36	0.03	292.87	66.08	5.80
0.736	0.00	0.00	15.85	0.39	0.04	341.46	72.00	5.92
0.858	0.00	0.00	18.48	0.49	0.10	398.11	77.85	5.85
1.00	0.00	0.00	21.54	0.73	0.24	464.16	83.43	5.58
1.17	0.00	0.00	25.12	1.22	0.50	541.17	88.51	5.08
1.36	0.00	0.00	29.29	2.12	0.90	630.96	92.88	4.37
1.58	0.00	0.00	34.15	3.55	1.43	735.64	96.35	3.47
1.85	0.00	0.00	39.81	5.63	2.08	857.70	98.76	2.41
2.15	0.00	0.00	46.42	8.41	2.78	1000.00	100.00	1.24

Preprints (www.preprints.org) | NOT PEER-REVIEWED | Posted: 31 October 2023 doi:10.20944/preprints202310.2036.v1

Figure A4. Statistical characteristics of the particle size distribution for p = 500 kPa.

Size (µm)	% V <	% V	Size (µm)	% V <	% V	Size (µm)	% V <	% V
0.117	0.00	0.00	2.51	0.00	0.00	54.12	45.17	9.74
0.136	0.00	0.00	2.93	0.01	0.01	63.10	55.17	9.99
0.158	0.00	0.00	3.41	0.05	0.04	73.56	64.72	9.56
0.185	0.00	0.00	3.98	0.15	0.10	85.77	73.27	8.54
0.215	0.00	0.00	4.64	0.30	0.16	100.00	80.41	7.14
0.251	0.00	0.00	5.41	0.53	0.22	116.59	86.00	5.60
0.293	0.00	0.00	6.31	0.80	0.28	135.94	90.13	4.13
0.341	0.00	0.00	7.36	1.11	0.31	158.49	93.01	2.88
0.398	0.00	0.00	8.58	1.43	0.32	184.79	94.95	1.94
0.464	0.00	0.00	10.00	1.74	0.32	215.44	96.24	1.29
0.541	0.00	0.00	11.66	2.07	0.33	251.19	97.12	0.88
0.631	0.00	0.00	13.59	2.49	0.41	292.87	97.76	0.64
0.736	0.00	0.00	15.85	3.12	0.63	341.46	98.26	0.50
0.858	0.00	0.00	18.48	4.20	1.08	398.11	98.69	0.42
1.00	0.00	0.00	21.54	6.02	1.82	464.16	99.05	0.36
1.17	0.00	0.00	25.12	8.92	2.90	541.17	99.35	0.30
1.36	0.00	0.00	29.29	13.21	4.29	630.96	99.60	0.25
1.58	0.00	0.00	34.15	19.09	5.88	735.64	99.79	0.19
1.85	0.00	0.00	39.81	26.58	7.49	857.70	99.93	0.14
2.15	0.00	0.00	46.42	35.43	8.85	1000.00	100.00	0.07

Figure A5. Statistical characteristics of the particle size distribution for p = 600 kPa.

Size (µm)	% V <	% V	Size (µm)	% V <	% V	Size (µm)	% V <	% V
0.117	0.00	0.00	2.51	0.00	0.00	54.12	23.94	8.22
0.136	0.00	0.00	2.93	0.00	0.00	63.10	32.90	8.96
0.158	0.00	0.00	3.41	0.00	0.00	73.56	41.66	8.76
0.185	0.00	0.00	3.98	0.00	0.00	85.77	49.37	7.71
0.215	0.00	0.00	4.64	0.00	0.00	100.00	55.46	6.10
0.251	0.00	0.00	5.41	0.00	0.00	116.59	59.78	4.32
0.293	0.00	0.00	6.31	0.00	0.00	135.94	62.55	2.76
0.341	0.00	0.00	7.36	0.00	0.00	158.49	64.26	1.72
0.398	0.00	0.00	8.58	0.00	0.00	184.79	65.57	1.30
0.464	0.00	0.00	10.00	0.00	0.00	215.44	67.07	1.50
0.541	0.00	0.00	11.66	0.00	0.00	251.19	69.25	2.18
0.631	0.00	0.00	13.59	0.00	0.00	292.87	72.36	3.11
0.736	0.00	0.00	15.85	0.00	0.00	341.46	76.38	4.01
0.858	0.00	0.00	18.48	0.00	0.00	398.11	81.00	4.62
1.00	0.00	0.00	21.54	0.00	0.00	464.16	85.79	4.79
1.17	0.00	0.00	25.12	0.14	0.14	541.17	90.29	4.50
1.36	0.00	0.00	29.29	1.37	1.23	630.96	94.12	3.84
1.58	0.00	0.00	34.15	4.22	2.85	735.64	97.08	2.95
1.85	0.00	0.00	39.81	9.01	4.79	857.70	99.04	1.97
2.15	0.00	0.00	46.42	15.72	6.71	1000.00	100.00	0.96

Figure A6. Statistical characteristics of the particle size distribution for p = 700 kPa.

Size (µm)	% V <	% V	Size (µm)	% V <	% V	Size (µm)	% V <	% V
0.117	0.00	0.00	2.51	0.00	0.00	54.12	28.59	9.74
0.136	0.00	0.00	2.93	0.00	0.00	63.10	38.95	10.36
0.158	0.00	0.00	3.41	0.00	0.00	73.56	48.75	9.80
0.185	0.00	0.00	3.98	0.00	0.00	85.77	56.99	8.24
0.215	0.00	0.00	4.64	0.00	0.00	100.00	63.06	6.07
0.251	0.00	0.00	5.41	0.00	0.00	116.59	66.87	3.82
0.293	0.00	0.00	6.31	0.00	0.00	135.94	68.82	1.94
0.341	0.00	0.00	7.36	0.00	0.00	158.49	69.57	0.76
0.398	0.00	0.00	8.58	0.00	0.00	184.79	69.92	0.34
0.464	0.00	0.00	10.00	0.00	0.00	215.44	70.52	0.60
0.541	0.00	0.00	11.66	0.00	0.00	251.19	71.90	1.38
0.631	0.00	0.00	13.59	0.00	0.00	292.87	74.33	2.43
0.736	0.00	0.00	15.85	0.00	0.00	341.46	77.77	3.44
0.858	0.00	0.00	18.48	0.00	0.00	398.11	81.92	4.15
1.00	0.00	0.00	21.54	0.00	0.00	464.16	86.34	4.42
1.17	0.00	0.00	25.12	0.07	0.07	541.17	90.57	4.23
1.36	0.00	0.00	29.29	1.50	1.43	630.96	94.24	3.67
1.58	0.00	0.00	34.15	4.95	3.45	735.64	97.11	2.87
1.85	0.00	0.00	39.81	10.76	5.82	857.70	99.05	1.94
2.15	0.00	0.00	46.42	18.85	8.09	1000.00	100.00	0.95

Figure A7. Statistical characteristics of the particle size distribution for p = 800 kPa.

Size (µm)	% V <	% V	Size (µm)	% V <	% V	Size (µm)	% V <	% V
0.117	0.00	0.00	2.51	0.00	0.00	54.12	28.20	13.92
0.136	0.00	0.00	2.93	0.00	0.00	63.10	44.69	16.49
0.158	0.00	0.00	3.41	0.00	0.00	73.56	59.60	14.90
0.185	0.00	0.00	3.98	0.00	0.00	85.77	69.79	10.19
0.215	0.00	0.00	4.64	0.00	0.00	100.00	74.88	5.09
0.251	0.00	0.00	5.41	0.00	0.00	116.59	76.59	1.71
0.293	0.00	0.00	6.31	0.00	0.00	135.94	76.90	0.31
0.341	0.00	0.00	7.36	0.00	0.00	158.49	76.92	0.02
0.398	0.00	0.00	8.58	0.00	0.00	184.79	76.92	0.00
0.464	0.00	0.00	10.00	0.00	0.00	215.44	76.92	0.00
0.541	0.00	0.00	11.66	0.00	0.00	251.19	77.41	0.49
0.631	0.00	0.00	13.59	0.00	0.00	292.87	79.53	2.12
0.736	0.00	0.00	15.85	0.00	0.00	341.46	83.56	4.03
0.858	0.00	0.00	18.48	0.00	0.00	398.11	88.56	5.00
1.00	0.00	0.00	21.54	0.00	0.00	464.16	93.18	4.62
1.17	0.00	0.00	25.12	0.00	0.00	541.17	96.58	3.40
1.36	0.00	0.00	29.29	0.17	0.17	630.96	98.61	2.03
1.58	0.00	0.00	34.15	1.38	1.21	735.64	99.59	0.97
1.85	0.00	0.00	39.81	5.43	4.06	857.70	99.93	0.35
2.15	0.00	0.00	46.42	14.28	8.85	1000.00	100.00	0.07

Figure A8. Statistical characteristics of the particle size distribution for p = 900 kPa.

References

1. Vasilyev, Yu.A., Domrina, E.S., Kaufman, S.V., & Maiorova, A.I. Classification of atomization devices. *Journal of Physics: Conference Series* **2019**, *1359*(1), 012131. DOI 10.1088/1742-6596/1359/1/012131
2. Gong, J., Fan, W., & Peng, J. Application analysis of hydraulic nozzle and rotary atomization sprayer on plant protection UAV. *International Journal of Precision Agricultural Aviation*, **2019**, *2*(1), 25-29. **DOI:** 10.33440/j.ijpaa.20190201.0021.
3. Alajmi, A., Alajmi, F., Alrashidi, A., Alrashidi, N., & Adam, N. M. Application of Ultrasonic Atomization on a Micro Jet Engine Using Biofuel for Improving Performance. *Processes* **2021**, *9*(11), 1963. **DOI:** 10.3390/pr9111963.
4. Thakur, P., Sonawane, S., Potoroko, I., & Sonawane, S. H. Recent advances in ultrasound-assisted synthesis of nano-emulsions and their industrial applications. *Current Pharmaceutical Biotechnology* **2021**, *22*(13), 1748-1758. **DOI:** 10.2174/1389201021666201104150102.
5. Zhang, Q., Fan, L., Wang, H., Han, H., Zhu, Z., Zhao, X., & Wang, Y. A review of physical and chemical methods to improve the performance of water for dust reduction. Process Safety and Environmental Protection **2022**, *166*, 86-98. **DOI:** 10.1016/j.psep.2022.07.06.
6. Putra, I. D. G. A. T., Sunu, P. W., Temaja, I. W., Sugiartha, N., Sugina, I. M., & Suirya, I. W. Investigation on application of ultrasonic humidifier for air conditioning system. *Journal of Physics: Conference Series* **2020**, *1450*(1), 012050. **DOI:** 10.1088/1742-6596/1450/1/012050.
7. Ardekani, S. R., Aghdam, A. S. R., Nazari, M., Bayat, A., Yazdani, E., & Saievar-Iranizad, E. A comprehensive review on ultrasonic spray pyrolysis technique: Mechanism, main parameters and applications in condensed matter. *Journal of Analytical and Applied Pyrolysis* **2019**, *141*, 104631. **DOI:** 10.1016/j.jaap.2019.104631.
8. Kustron, P., Korzeniowski, M., Sajbura, A., Piwowarczyk, T., Kaczynski, P., & Sokolowski, P. Development of High-Power Ultrasonic System Dedicated to Metal Powder Atomization. *Applied Sciences* **2023**, *13*(15), 8984. **DOI:** 10.3390/app13158984.
9. Guerra-Bravo, E.; Lee, H.-J.; Baltazar, A.; Loh, K.J. Vibration Analysis of a Piezoelectric Ultrasonic Atomizer to Control Atomization Rate. *Applied Sciences* 2021, *11*, 8350. **DOI:** 10.3390/app11188350.
10. Ramisetty, K.A.; Pandit, A.B.; Gogate, P.R. Investigations into Ultrasound Induced Atomization. *Ultrason. Sonochemistry* **2013**, *20*, 254–264. **DOI:** 10.1016/j.ultsonch.2012.05.001.
11. Khmelev, V.N., Shalunov, A.V., Khmelev, S.S., & Tsyganok, S.N. *Ultrasound. Devices and technologies: monograph*; Alt Publishing House tech. un-t: Biysk, Russia, 2015. (In Russ.).
12. Rosenberg, L. D. *Physical foundations of ultrasonic technology.* Nauka: Moscow, Russia, 1970. (In Russ.).
13. Kedrinsky, V. K. Hydrodynamics of explosion. *Applied mechanics and technical physics* **1987**, *28*(4), 491-515.
14. Kudryashova, O. B., Muravlev, E. V., & Vorozhtsov, B. I. Generation of a Fine Aerosol in a Cavitation Regime. *Journal of Engineering Physics and Thermophysics* **2020**, *93*, 1138-1146.
15. Lang, R. J. Ultrasonic atomization of liquids. *The journal of the acoustical society of America* **1962**, 34(1), 6-8.
16. Pages, D. G., & Galustov, V. S. *Fundamentals of liquid spraying technique*. Chemistry: Moscow, Russia, 1984 (In Russ.).